World Journal of Stem Cells

Submit a Manuscript: https://www.f6publishing.com

World J Stem Cells 2025 October 26; 17(10): 109284

DOI: 10.4252/wjsc.v17.i10.109284

ISSN 1948-0210 (online)

ORIGINAL ARTICLE

Basic Study

Melanoma cell adhesion molecule-positive mesenchymal stromal cells alleviate acute respiratory distress syndrome *via* nuclear factor kappa-B-mediated paracrine regulation

Ya-Li Zhang, Ding-Ke Wen, Sheng-Nan Wang, Yi Tan, He-Ran Ma

Specialty type: Cell and tissue engineering

Provenance and peer review: Unsolicited article; Externally peer reviewed.

Peer-review model: Single blind

Peer-review report's classification

Scientific Quality: Grade A, Grade A, Grade C, Grade C, Grade D

Novelty: Grade B, Grade B, Grade B, Grade C, Grade C

Creativity or Innovation: Grade A, Grade B, Grade C, Grade C, Grade D

Scientific Significance: Grade A, Grade B, Grade C, Grade C, Grade D

P-Reviewer: Eid N, MD, PhD, Associate Professor, Malaysia; Iglesias J, Associate Professor, Consultant, United States; Yang C, PhD, Professor, China

Received: May 8, 2025

Revised: June 24, 2025

Accepted: August 27, 2025

Published online: October 26, 2025

Processing time: 171 Days and 0.5 Hours

Ya-Li Zhang, Ding-Ke Wen, Sheng-Nan Wang, Yi Tan, He-Ran Ma, Department of Research and Development, Qilu Cell Therapy Technology Co., Ltd, Jinan 250000, Shandong Province, China

Co-corresponding authors: Yi Tan and He-Ran Ma.

Corresponding author: He-Ran Ma, PhD, Department of Research and Development, Qilu Cell Therapy Technology Co., Ltd, No. 6 Gangyuan Road, Licheng District, Jinan 250000, Shandong Province, China. maheran@yinfeng.com.cn

Abstract

BACKGROUND

Mesenchymal stromal cells (MSCs) are renowned for their immunosuppressive properties, which make them widely used in managing excessive inflammation. Although CD146+ and CD146- MSCs exhibit similar morphological traits and surface marker expression levels, the specific characteristics and differential regulatory mechanisms of these two subtypes remain poorly understood. This knowledge gap has limited the precise application of MSCs in targeted therapeutic strategies.

AIM

To compare the functional differences between CD146+ and CD146- MSCs and investigate the underlying mechanisms.

METHODS

In this study, magnetic beads were used to sort umbilical cord-derived MSCs into CD146+ and CD146- subsets. The pro-angiogenic factors (hepatocyte growth factor, prostaglandin E2, vascular endothelial growth factor, angiopoietin-1) production and immunomodulatory effects on T lymphocyte subsets were evaluated *in vitro*. The therapeutic efficacy was assessed in an acute respiratory distress syndrome (ARDS) mouse model *via* tail vein injection.

RESULTS

Cytokine secretion and angiogenesis: CD146+ MSCs significantly increased the production of hepatocyte growth factor, prostaglandin E2, vascular endothelial growth factor, and angiopoietin-1 and exhibited increased pro-angiogenic activity

in vitro. Immunomodulatory effects: CD146+ MSCs potently inhibited the differentiation and proliferation of pro-inflammatory T helper type 1/T helper type 17 cells while promoting the expansion of regulatory T cells during T lymphocyte activation. ARDS therapy: In a mouse ARDS model, compared with CD146- MSCs, CD146+ MSCs demonstrated superior therapeutic efficacy, as evidenced by improved clinical scores. Mechanistically, CD146+ MSCs activated the nuclear factor kappa B pathway, upregulated cyclooxygenase 2 expression, and facilitated damaged epithelial cell repair.

CONCLUSION

CD146+ MSCs show stronger ARDS therapeutic potential than CD146- MSCs *via* pro-angiogenic/immunomodulatory traits. Nuclear factor kappa B/cyclooxygenase 2 activation aids epithelial repair, highlighting CD146+ MSCs as promising targets.

Key Words: Mesenchymal stromal cells; Melanoma cell adhesion molecule; Acute respiratory distress syndrome; Nuclear factor kappa B; CD146

Core Tip: Mesenchymal stromal cells (MSCs) are recognized for their immunosuppressive properties and are widely used to control excessive inflammation. This study demonstrated that, compared with CD146- MSCs, CD146+ MSCs exhibit greater secretion of pro-angiogenic factors and enhanced anti-inflammatory and immunomodulatory capacities. CD146+ MSCs repair epithelial cells by activating the nuclear factor kappa B/cyclooxygenase 2 pathway, thereby exerting superior therapeutic efficacy in the treatment of acute respiratory distress syndrome.

Citation: Zhang YL, Wen DK, Wang SN, Tan Y, Ma HR. Melanoma cell adhesion molecule-positive mesenchymal stromal cells alleviate acute respiratory distress syndrome *via* nuclear factor kappa-B-mediated paracrine regulation. *World J Stem Cells* 2025; 17(10): 109284
URL: https://www.wjgnet.com/1948-0210/full/v17/i10/109284.htm
DOI: https://dx.doi.org/10.4252/wjsc.v17.i10.109284

INTRODUCTION

Mesenchymal stem cells (MSCs) are increasingly utilized in biomedical applications. Since MSCs do not express histocompatibility complexes or immunostimulatory molecules, are not detected by immune surveillance, and do not provoke graft rejection after transplantation, making them highly promising for biomedical use, particularly in tissue engineering[1]. At present, MSCs are also widely applied in the treatment of various tissue degenerative diseases and injury repair[2-4]. In 2006, the International Society for Cell Therapy defined MSCs, emphasizing the expression of the surface markers CD73, CD90, and CD105 in more than 95% of cells, whereas markers such as CD45, CD34, CD14, CD11b, CD79α, CD19, and HLA-DR are absent[5]. However, none of these markers are unique to MSCs. While MSCs show significant potential, differences in their origin, individual sources, and environmental conditions contribute to their heterogeneity. Increasing evidence suggests that MSCs represent a heterogeneous group, with variations in surface marker expression linked to distinct cytological characteristics and functions[6]. Despite their potential, the clinical application of MSCs to treat certain disorders is limited by the heterogeneity of cell subsets and regenerative capacity. As such, there is an urgent need for precision therapy in MSC applications.

Owing to their heterogeneous nature, MSCs express different surface markers and exhibit distinct biological properties. As a result, isolating and identifying specific MSC subsets from different sources to evaluate their therapeutic efficacy for particular disorders is a key focus for future precision stem cell therapies. Various studies have isolated MSC subpopulations, such as those expressing CD146, CD106, Stro-1, SSEA-4, and CD271, to investigate their functions and biological characteristics[7,8].

CD146, also referred to as melanoma cell adhesion molecule, is a membrane glycoprotein that belongs to the immunoglobulin gene superfamily and was first identified in human melanoma cells[9]. It is particularly useful for identifying authentic MSCs, as it is widely distributed across the vascular network and plays a key role in angiogenesis and endothelial cell activity[10-12]. Additionally, CD146 is highly expressed in various cell types, including smooth muscle and vascular endothelial cells[13]. In regenerative medicine, the CD146+ MSC subset has shown enhanced biological functionality and therapeutic potential[14]. CD146 is detectable in bone marrow derived MSCs (BM-MSCs) and MSCs derived from various sources, such as adipose tissue, synovium, umbilical cord (UC), UC blood, placenta, dermis, periodontal ligament, and intervertebral discs. Notably, CD146+ BM-MSCs exhibit stronger migratory and homing abilities[15,16], as well as enhanced immunosuppressive and cytokine secretion functions[17]. CD146+ MSCs from adipose tissue demonstrate superior proliferation and angiogenesis capabilities[18-20], whereas those from dental pulp tissue show increased osteogenic differentiation potential[21]. Additionally, CD146+ MSCs exhibit lower heterogeneity [22], indicating that CD146+ MSCs cultured *in vitro* possess greater stemness and primitive characteristics.

Despite its promise, the molecular pathways regulated by CD146 in MSCs remain insufficiently understood. In this study, we aimed to examine how CD146 influences MSC effects and to explore the underlying mechanisms thereof. Our findings indicate that CD146+ MSCs can repair damaged lung epithelial cells and more effectively treat acute respiratory distress syndrome (ARDS) in mice. Mechanistically, CD146+ MSCs increase cyclooxygenase 2 (COX2) expression by activating the nuclear factor kappa B (NF-κB) pathway. These results emphasize the potential of CD146+ MSCs for ARDS treatment and provide insights into strategies to improve the therapeutic potential of MSCs.

MATERIALS AND METHODS

Main material

The BM-MSC serum-free medium used in cell cultures was supplied by Dakewe Biotech Co. in China (DY culture medium), while the BM-MSC serum-free medium was obtained from Shandong Qilu Cell Therapy Engineering Technology Co. Ltd in China (YF culture medium). Additionally, 3D FloTrix MSCs in serum-free medium were provided by Cytoniche in China (HK culture medium). Cell culture reagents (RPMI 1640 medium, DMEM and fetal bovine serum) were obtained from Gibco Co. (Grand Island, NY, United States).

The following antibodies were purchased from Cell Signaling Technology (MA, United States): Phospho-NF-κB (#3031), NF-κB (#8242), protein kinase A (PKA) (#4782), phospho-PKA (p-PKA) (#4781), cyclic-AMP response element-binding protein (CREB) (#9197), phospho-CREB (#9198), zonula occludens-1 (ZO-1) (#5406), COX2 (#4842) and VE-cadherin (#2158). The FITC Annexin V Apoptosis Detection Kit with propidium iodide (PI) (C1062M) was obtained from Beyotime in China. The anti-GAPDH antibody (#ab20272) was acquired from Abcam in United Kingdom. Caffeic acid phenethyl ester (CAPE, S7414) was purchased from Selleck (TX, United States).

Four-week-old male BALB/c mice were obtained from the Laboratory Animal Centre of Beijing Vital River Laboratory Animal Technology Co., Ltd. All the animal experiments were conducted in accordance with laboratory animal care guidelines, and the experimental protocols were approved by the Biomedical Research Ethics Committee of the Institute of Biophysics, Chinese Academy of Sciences (Beijing, China). All the mouse experiments were performed without blinding and were conducted in accordance with the Public Health Service Policy on Humane Care and Use of Laboratory Animals. The Experimental Animal Ethics Committee of Army Medical University approved the experiments, and the ethical approval number was No. AMUWEC20210830.

Cell lines and cell culture

Human UC derived MSCs (UCMSCs) were obtained from Shandong Qilu Cell Therapy Engineering Technology Co. Ltd. The source, screening, and collection process of human UCs at Yantai Yuhuangding Hospital Affiliated with Qingdao University met the national ethical requirements, and the ethical approval number was No. [2021]003. Moreover, the participants signed an informed consent form before participation.

In brief, UCs were obtained from patients who consented to deliver a full-term infant *via* cesarean section. After the arteries and veins of the UC were removed, the UC was cut as finely as possible with sterile surgical scissors, preferably no more than 1 mm in size. The UC fragments were resuspended in MSC serum-free medium, and the suspension was subsequently transferred to cell culture flasks and incubated at 37 °C in a 5% CO_2 environment. After the cells had climbed, the medium was changed every 2 days. When the cells reached 80% to 90% confluence, they were harvested and frozen at -80 °C until use in the experiments.

The pathogenesis of ARDS involves multiple factors, including inflammatory disorders, alveolar epithelial cell injury, pulmonary capillary endothelial cell injury, microcirculatory disorders, and cell apoptosis. One of the core pathological features of ARDS is the destruction of the alveolar-capillary barrier. Pulmonary microvascular endothelial cells are important components of the alveolar-capillary barrier, whereas type II alveolar epithelial cells are another key component of the alveolar barrier and are responsible for secreting surfactant, maintaining the alveolar fluid balance, and participating in epithelial repair[23-25]. To explore the repair mechanism, we selected alveolar epithelial cells and pulmonary capillary endothelial cells as experimental subjects. Human lung microvascular endothelial cells (HULEC-5a) and human type II alveolar epithelial cells (HPAEpic-II-SV40) were purchased from Zhejiang Meisen Cell Technology Co., Ltd., in 2024. Both cell lines were verified by suppliers. Following the experiments, polymerase chain reaction (PCR) was performed to ensure the absence of mycoplasma contamination. The cells were cultured in DMEM (Gibco Life Technologies, NY, United States) containing 10% fetal bovine serum and 1% penicillin-streptomycin (Gibco, NY, United States) at 37 °C and 5% CO_2.

Isolation and identification of CD146-producing stem cells

The EasySep™ Release Human PE Positive Selection Kit (catalog #17654, STEMCELL, Canada) was used to isolate and separate CD146+ cells from human UCMSCs. PE-conjugated anti-CD146 antibody (361006, Biolegend, CA, United States) was then used to sort CD146+ cells, with 12%-32% of the UCMSCs identified as CD146+. Cell separation followed the EasySep™ protocol. Briefly, the cells were incubated for 30 minutes with an anti-CD146 antibody at room temperature. The selection cocktail was then added, and the sample was incubated for 5 minutes at ambient temperature. RapidSpheres™ was added for an additional 5 minutes of incubation at room temperature, after which the sample was sorted *via* FasySen™ (catalog #18000, STEMCELL, Canada). The sorted cells were subsequently cultured in a growth medium as described. MSCs were collected at passages 5-6 for further analysis.

Reverse transcription-quantitative PCR

RNA was extracted from cells *via* a TRIzol kit (TaKaRa, Shiga, Japan). For cDNA synthesis, 1 μg of RNA was reverse transcribed *via* the PrimeScript RT reagent Kit (TaKaRa, Shiga, Japan). Quantitative PCR (qPCR) was subsequently performed to quantify cDNA *via* a SYBR Green real-time quantitative PCR kit (TaKaRa, Shiga, Japan), with GAPDH used as the endogenous reference. The following primers (GenScript, NJ, United States) were used for qPCR: *COX2* forward: 5′-AGGACTCTGCTCACGAAGGA-3′ and reverse: 5′-TGACATGGATTGGAACAGCA-3′; *GAPDH* forward: 5′-ACCCTTAAGAGGGATGCTGC-3′ and reverse: 5′-CCCAATACGGCCAAATCCGT-3′. The short hairpin RNA (shRNA) NF-κB (shNF-κB) sequence (5′-3′) was as follows: 5′-GGACCTACGAGACCTTCAA-3′. Each sample was tested in triplicate. Gene expression was calculated using the $2^{-\Delta\Delta Ct}$ method from three independent assays.

Western blotting

For western blotting, cell lysis was performed with RIPA buffer containing a protease inhibitor cocktail, as previously described. Protein concentrations were determined using Enhanced BCA Protein Assay Reagent (Beyotime, Jiangsu, China). The proteins were separated by 10% sodium-dodecyl sulfate gel electrophoresis and transferred to polyvinylidene fluoride membranes (Bio-Rad, 162-0177, CA, United States). The membranes were blocked with 5% nonfat dry milk and then incubated with the primary antibody overnight at 4 °C, followed by a 2-hour incubation with HRP-labeled secondary antibody at room temperature. The protein bands were detected *via* an enhanced chemiluminescence system (Perkin-Elmer Life Sciences, Boston, MA, United States). Band intensities were analyzed with ImageJ software, with GAPDH used as the internal control.

Cord formation assays

The 96-well plates were coated with growth factor-reduced Matrigel (BD Biosciences, CA, United States) and allowed to polymerize for 30 minutes at 37 °C. For coculture experiments, human umbilical vein endothelial cells (C2517A, Lonza, MD, United States) (3×10^4/well) and CD146+/- MSCs (1000/well) were seeded simultaneously onto polymerized Matrigel. After 5 hours of culture in DMEM, cord formation was monitored *via* microscopy by examining seven randomly chosen fields at 7 × magnification (IX71, Olympus, Japan). The analysis included measurements of cord length per field of view and branch points. Three replicate wells and images were used for each group.

Phenotype analysis of T-cell subsets

For T-cell subset phenotype analysis, CD146+/- MSCs (2×10^5/well) were plated in 12-well plates with RPMI1640 containing 10% fetal bovine serum (1 mL per well) and three wells per group. After 24 hours of culture, 1×10^6 peripheral blood mononuclear cells were added to each well at a 5:1 ratio of peripheral blood mononuclear cells to MSCs, followed by overnight incubation for 18 hours. T helper type 1 (Th1) /T helper type 17 (Th17) cells were assessed by flow cytometry after treatment with PIB [PMA (50 ng/mL), Iono (1 μg/mL), or BFA (10 μg/mL)] for 6 hours. Regulatory T (Treg) cells were cocultured for 5 days without PIB supplementation. Flow cytometry was used to detect the proportions of Th1 (CD3+/CD8-/interferon-γ+), Th17 [CD3+/CD8-/interleukin (IL)-17A+], and Treg cells (CD4+CD25+/FoxP3+).

Cell apoptosis assay

Flow cytometry was utilized to assess cell apoptosis through Annexin V-FITC and PI double-staining, following established protocols (Beyotime, Shanghai, China). Briefly, 5 μL of Annexin V-FITC and 10 μL of PI (50 μg/mL) in 1 × binding buffer were added to stain 1×10^6 cells in the dark for 15 minutes at room temperature. A FACScan flow cytometer was used to measure the number of apoptotic cells, and FlowJo software was used for analysis. The cells were considered apoptotic if they were stained with Annexin V-FITC and/or PI. Each experiment was conducted in triplicate.

Cell permeability assessment

Endothelial permeability was measured in 6-well plates with 24 transwell inserts following specific protocols. After resuspension, CD146+ MSCs and CD146+ MSCs + CAPE (5 μmol/L) were seeded at 4×10^5 cells per well, and transwell inserts (0.48 μm) were seeded at 2×10^5 cells per well. HULEC-5a/HPAEpic-II-SV40 cells were resuscitated, forming a dense monolayer after 24 hours of culture. HULEC-5a/HPAEpic-II-SV40 cells were cocultured with MSCs, and the medium was replaced with lipopolysaccharide (LPS) (50 μg/mL) and 2% fetal bovine serum. After 48 hours of culture, the medium in the transwell inserts was carefully removed. FluoroBrite DMEM containing 100 μg/mL FITC-dextran (MW 40000) was added to the top chamber, and 2.5 mL of FluoroBrite DMEM was added to the bottom chamber. After 1 hour of incubation, the fluorescence intensity of the transwell culture medium was measured *via* a multifunctional enzyme-labeling assay. The permeability assay was repeated three times for each time point with three samples. For dose

conversion related to cell density, 5 μg of LPS corresponds to 1 × 10^6 cells (10^6 cells/mL).

mRNA sequencing and functional enrichment analysis

mRNA sequencing was performed to examine differentially expressed genes (DEGs) in CD146+ MSCs and CD146- MSCs using BMKCloud (http://www.biocloud.net). The DESeq2 R package (1.26.0) was employed to identify significant DEGs in both groups, applying thresholds of adjusted $P < 0.05$ and $|\log2 \text{ (fold change)}| > 1$. Heatmap version 1.0.10 was used for the generation of the heatmap. Kyoto Encyclopedia of Genes and Genomes analysis was conducted to identify pathways enriched by DEGs using the clusterProfiler R package (v3.13.0), with a significance threshold of $P < 0.05$. Furthermore, gene set enrichment analysis was performed using gene set enrichment analysis software (v2.2.3, http://software.broadinstitute.org/gsea/downloads.jsp) and MSigDB-curated gene sets (c2.cp.kegg.v6.2.symbols.gmt).

Cells treated with CAPE

CAPE was dissolved in DMSO to prepare a 10 mmol/L stock solution. For the experiments, the solution was diluted to a working concentration of 5 μM in serum-free medium, with a final DMSO concentration ≤ 0.1%. The control group was supplemented with an equal volume of DMSO simultaneously. The cells were pretreated with starvation medium for 1 hour, followed by incubation with CAPE for 24 hours, and control groups were established accordingly[26,27].

CD146+ MSCs were treated with caffeolate phenylethyl (CAPE) at a concentration of 5 μmol/L (Supplementary Figure 1). After 24 hours of CAPE treatment, *COX2* mRNA expression was assessed *via* reverse transcription-qPCR, and COX2, p-NF-κB, and signal transducer and activator of transcription 5 protein levels were evaluated using western blotting. Additionally, the secretion levels of the cytokines hepatocyte growth factor (HGF)/prostaglandin E2 (PGE2)/angiopoietin-1 (Ang-1) and vascular endothelial growth factor (VEGF) by CD146+ MSCs were measured using enzyme-linked immunosorbent assay (ELISA). Each assay was performed in triplicate.

Construction of stable NF-κB-knockdown cell lines

Lentiviral vectors encoding three different shRNAs, targeting human NF-κB {named as shNF-κB [shNF-κB(p65)]}, were purchased from Shanghai Genechem of China (Shanghai, China). CD146+ MSCs were transfected with the shSENP1 Lentivirus or empty lentiviral vector (named shCon) with polybrene (8 μg/mL, Sigma-Aldrich, MO, United States). The transfected cells were then subjected to selection with puromycin (3.0 μg/mL) for 4-5 days. Knockdown of NF-κB in stable cells was verified by reverse transcription-qPCR and western blotting.

Establishment of the ARDS model (in vivo)

A total of 50 mice were selected for test A, and another 50 were selected for test B. The mice were randomly divided into 5 groups on the basis of body weight: Normal control and model control (MG). After the ARDS model was established, MSCs cultured in media from different brands were injected *via* the caudal vein to form different groups: The DY group, the YF group, and the HK group (Figure 1A and Supplementary Figure 2).

The mice were fasted overnight but were allowed to drink water. All groups, except for the normal control group, received an LPS solution injected into the trachea to establish the ARDS model. Anesthesia was induced by intraperitoneal injection of tribromoethanol solution. After anesthesia, a tracheal intubation operating table was used to suspend the upper teeth of each mouse and extend its tongue. The glottic fissure was located with the aid of a lamp, and a tracheal drug delivery hose was inserted through it into the trachea. LPS solution (7 mg/kg) was administered *via* a pipette gun into the hose as the mouse breathed naturally[25,28,29]. Additionally, either 0.9% sodium chloride or MSCs (5 × 10^6 cells/kg) were administered once within 1 hour after modeling and again at 24 hours after tail vein injection (Figure 1A).

Lung wet-dry ratio, hematoxylin and eosin staining, and pathological score

On the dissection day of experiment A, the mice in test A were weighed to determine the differences between the groups. At 48 hours post-administration, the test A mice were euthanized *via* the cervical dislocation method, followed by lung removal. The right lung weights were recorded initially, after which the lungs were dried in a 37 °C electric blast drying oven for 24 hours before being reweighed. This allowed for the calculation of the wet-dry weight ratios of the right lungs for each mouse in the experimental groups. ZO-1 and VE-cadherin expression in lung tissue was measured *via* immunohistochemistry, with 5 animals in each group. The experiments were performed without blinding and in compliance with the Public Health Service Policy on Humane Care and Use of Laboratory Animals.

Bronchoalveolar lavage fluid blood cell tests and ELISA

Bronchoalveolar lavage fluid (BALF) was collected from test B mice 48 hours after administration. 500 μL/BALF was retrieved, and the white blood cell count was determined using an automatic blood cell analyzer. The remaining BALF was centrifuged at 1500 rpm for 5 minutes at 4 °C to separate the supernatants. The levels of IL-6, IL-1β, and tumor necrosis factor (TNF)-α in the supernatants were then measured using ELISA kits following the manufacturer's instructions. A multifunctional enzyme marker was used to detect cytokine levels in the supernatants following centrifugation of the BALF.

Lung tissue injury grade and pathological scoring in mice via hematoxylin and eosin staining

After 48 hours of fixation in 10% formalin, the mouse lung tissues were subjected to gradient ethanol dehydration, wax impregnation, slicing, deparaffinization by baking, hematoxylin and eosin staining, and rubber sealing. The tissues were then examined and photographed under a microscope. The pathological changes in the lung tissue of each group were assessed. On the basis of the extent of lung tissue damage, including congestion, alveolar cavity destruction, thickening of

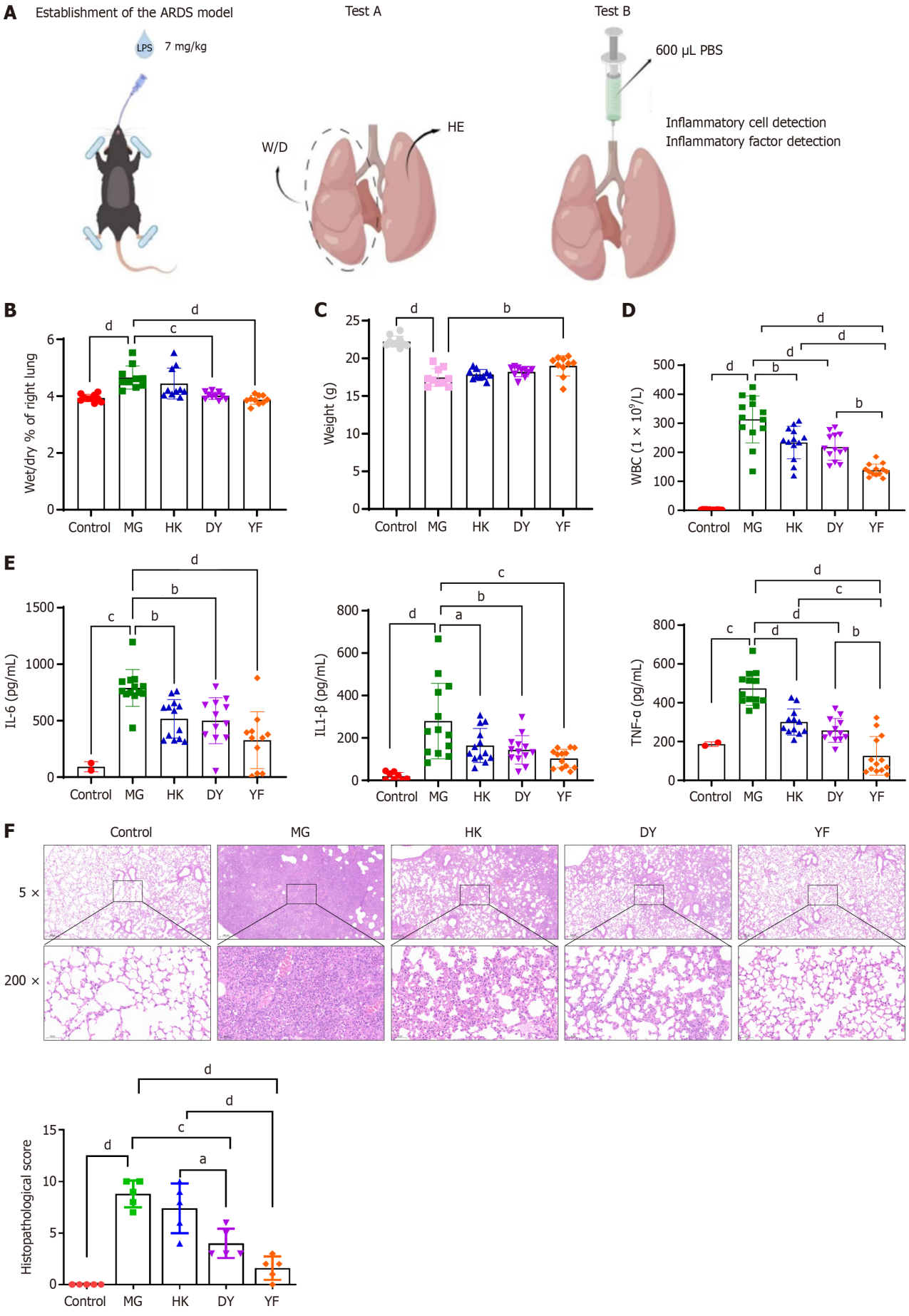

Figure 1 Effects of mesenchymal stromal cells in various media on acute respiratory distress syndrome. A: Diagram illustrating the acute

respiratory distress syndrome study design; B and C: Comparison of the wet-dry ratio (B) and body weight (C) of lung tissue from different groups; D and E: Cytokine levels in bronchoalveolar lavage fluid were measured at the experimental endpoint; F: Pathological changes and lung injury scores of the lung tissue in each group. The data are presented as means ± SD. Statistical analysis between groups was performed *via* two-sided Student's *t* test, and within groups, ANOVA was used for normally distributed data. $n = 10$, $^{a}P < 0.05$, $^{b}P < 0.01$, $^{c}P < 0.001$, $^{d}P < 0.0001$. ARDS: Acute respiratory distress syndrome; W/D: Wet-dry ratio; HE: Hematoxylin and eosin; PBS: Phosphate buffered saline; MG: Model control (vehicle administered *via* caudal vein injection after establishing the acute respiratory distress syndrome model; DY: Mesenchymal stromal cells cultured in medium from Dakewe Biotech Co., administered *via* caudal vein injection after establishing the acute respiratory distress syndrome model; YF: Mesenchymal stromal cells cultured in medium from Shandong Qilu Cell Therapy Engineering Technology Co. Ltd., administered *via* caudal vein injection under the acute respiratory distress syndrome model; HK: Mesenchymal stromal cells cultured in medium from Cytoniche, administered *via* caudal vein injection in the acute respiratory distress syndrome model; WBC: White blood cell; IL: Interleukin; TNF: Tumor necrosis factor.

the alveolar walls, and neutrophil infiltration, lung injury was classified into five levels: 0 (no injury), 1 (< 25% injury), 2 (25%-50% injury), 3 (50%-75% injury), and 4 (> 75% injury). The acute lung injury/ARDS pathological score was calculated by summing the individual lesion scores, with higher values indicating more severe injury.

Immunohistochemical staining

Immunohistochemistry was performed to assess VE-cadherin and ZO-1 expression, as previously described[30]. Briefly, tissue samples were fixed in formalin, embedded in paraffin, and then sectioned into 4-μm slices, followed by deparaffinization with xylene and rehydration with alcohol. After antigen retrieval, the sections were incubated with anti-VE-cadherin and anti-ZO-1 primary antibodies at 4 °C for 24 hours. After rinsing with phosphate buffered saline, the sections were incubated for 1 hour at room temperature with peroxidase-labeled goat anti-human/mouse secondary antibodies (1:300). Five random fields per section were selected and observed under a light microscope (100X, BX51, Olympus, Japan) *via* a digital camera (DP72, Olympus, Japan). VE-cadherin and ZO-1 expression levels were quantified *via* the histochemistry score (H-score), which was calculated by multiplying the percentage of positive cells (PI) by the staining intensity (i+1).

Statistical analysis

Data normality was assessed using the Shapiro–Wilk test. Continuous outcomes were reported as mean ± SEM. For comparisons of gene expression levels, unpaired *t* tests were used. Differences in histological measurements across multiple groups were analyzed using one-way analysis of variance (ANOVA), followed by the Holm–Šidák method to correct for multiple comparisons and control the familywise type I error rate. Statistical significance was interpreted at four levels: $P < 0.05$, $P < 0.01$, $P < 0.001$, and $P < 0.0001$. All statistical analyses were conducted using GraphPad Prism software (version 9.0; GraphPad, Inc., La Jolla, CA, United States).

RESULTS

Differential therapeutic effects of MSCs cultured in different media on lung function and pathology in ARDS mice

The right lungs of the mice in experiment A were dissected to determine the ratio of dry to wet weight of the right lung in each group. The ratio of the right lung in the MG group was significantly greater than that in the normal control group ($^{d}P < 0.0001$), indicating that LPS induced pulmonary edema in the model mice. Compared with that in the MG group, the wet-to-dry weight ratio of the right lung in each treatment group was significantly lower (Figure 1B, HK *vs* MG: No significance; DY *vs* MG: $^{c}P < 0.001$; YF *vs* MG: $^{d}P < 0.0001$). These results suggested that MSCs from different groups could reduce ARDS-induced edema to a certain extent.

Mouse weights were recorded on the necropsy day (Figure 1C). Compared with the normal control group, the MG group presented significant weight loss ($^{d}P < 0.0001$), indicating that the LPS model caused weight reduction in the mice. In comparison, the YF treatment group presented a noticeable increase in weight compared with the MG group ($^{b}P < 0.01$). Although weight increases were observed in the other treatment groups, no statistically significant differences were found.

Alveolar lavage fluid was collected from the mice in group B to examine changes in white blood cell counts. Compared with the normal control group, the MG group presented a significant increase in leukocyte number ($^{c}P < 0.001$), whereas all the treatment groups presented a noticeable reduction in leukocyte count compared with the MG group ($^{b}P < 0.01$, $^{d}P < 0.0001$), with the YF treatment group showing the lowest leukocyte count (Figure 1D). These findings suggest that various MSC treatments can partially reduce the number of inflammatory cells in the BALF of model mice. Furthermore, the IL-1β, IL-6, and TNF-α levels in the BALF were significantly elevated compared with those in the control group ($^{c}P < 0.001$, $^{d}P < 0.0001$). Compared with those in the model group, the IL-1β levels were notably lower in the treatment groups, with the YF treatment group showing the lowest levels. These findings indicate that MSC treatments may help reduce the expression of inflammatory cytokines (Figure 1E).

Pathological analysis revealed that the control group had a well-preserved lung structure, clear alveolar cavities, and no signs of hyperemia, edema, or inflammatory cell infiltration in the alveolar walls. Conversely, the model group exhibited damaged alveolar structure, with hyperemia and edema in the alveolar walls, accompanied by inflammatory cell infiltration, indicating significant lung injury. Compared with that in the model group, lung tissue damage in the treatment groups was less severe (Figure 1F). The treatment effect in the YF group was the greatest. MG: Vehicle administered *via* caudal vein injection after establishing the ARDS model; DY: MSCs cultured in medium from Dakewe

Biotech Co., administered *via* caudal vein injection after establishing the ARDS model; YF: MSCs cultured in medium from Shandong Qilu Cell Therapy Engineering Technology Co. Ltd., administered *via* caudal vein injection under the same model; HK: MSCs cultured in medium from Cytoniche, administered *via* caudal vein injection in the ARDS model.

CD146 expression was significantly increased in the YF culture system

To determine which cell subsets in the YF culture system contribute to the improved effectiveness of MSCs in ARDS treatment, flow cytometry was employed to analyze protein changes. The findings revealed a significant increase in CD146 expression following culture in the YF system (Figure 2).

Biological characteristics of UC-CD146+/- MSCs

CD146+/- MSCs were separated *via* an immune magnetic bead system, and flow cytometry was performed to evaluate cell purity. Prior to separation, CD146+ MSCs typically represented 33.9%-81.3% of the population (Figure 3A). To assess immunomodulatory activity, BM-MSCs were inflammatory primed to initiate a response, followed by profiling of the secreted proteins and detection of transcriptional changes. The secretion levels of HGF, PGE-2, VEGF, and Ang-1 in both MSC subsets under different conditions were then measured *via* ELISA. The results indicated that the secretion of these factors was significantly greater in the CD146+ MSCs than in the CD146- MSCs (Figure 3B).

To compare the angiogenic ability of CD146+ MSCs and CD146- MSCs, the tubular structure of human UCMSCs was detected *via* Matrigel, and the results are shown in Figure 3. The morphology of the CD146- MSCs was spindle shaped and polygonal, and few cells formed processes. The connections between the cells were incomplete, and the CD146-MSCs could not form lumen-like structures. The other two groups of cells could form cell-cell connections and complete lumen-like structures. Among them, the combined induction group formed more lumen-like structures and cross-linked with each other to form a network structure, as shown in Figure 3C. ImageJ software was used to analyze the number of tubes and nodes formed by the cells, and the results revealed that the number in the CD146+ MSC group was significantly greater than that in the CD146- MSC group; moreover, the number in the CD146+ MSC group was significantly greater than that in the unsorted MSC group.

Immunomodulation of CD146+ MSCs and CD146- MSCs

In the study of MSC immunoregulation, dynamic changes in T-cell subsets (such as Th1/Th17/Treg) are key indicators for evaluating immune balance[31-33]. MSCs exert immunomodulatory effects by inhibiting the differentiation of Th1 and Th17 cells (pro-inflammatory) and promoting the differentiation of Tregs (immunosuppressive). Therefore, in this study, the proportions of Th1 (CD3+/CD8-/interferon-γ+), Th17 (CD3+/CD8-/IL-17A+), and Treg (CD4+/CD25+/FoxP3+) cells were determined to verify the regulatory effect of CD146+/- MSCs on the direction of T-cell differentiation at the cellular phenotype level. Compared with the CD146- MSC coculture, the CD146+ MSC coculture more effectively inhibited Th1/Th17 cells and promoted Treg cells activation *in vitro* ($^{d}P < 0.0001$) (Figure 3D).

CD146+ MSCs have better therapeutic effects in ARDS

The therapeutic effect of CD146+ MSCs was further assessed in an LPS-induced ARDS model. Various cell subpopulations were injected into the mouse abdominal cavity, and after 48 hours, the CD146+ MSC group showed notable improvements in body weight, wet-dry weight ratios, and white blood cell count (Figure 4A-C). Histological staining (Figure 4D and E) revealed lung damage in ARDS mice treated with CD146+/- MSCs. The pathological scores were greater in the CD146- MSC group than in the saline or CD146+ MSC groups. Moreover, VE-cadherin and ZO-1 protein levels were significantly greater in the CD146+ MSC group than in the CD146- MSC group (Figure 4F and G), corroborating the results of the *in vitro* analyses.

CD146+ MSCs promote COX2 expression via the NF-κB signaling pathway

To explore the mechanism underlying the function of CD146 in MSCs, CD146+ MSCs and CD146- MSCs were subjected to mRNA sequencing after sorting. As depicted in Figure 5A, a significant number of DEGs were observed between the CD146+ MSC and CD146- MSC groups. Kyoto Encyclopedia of Genes and Genomes analysis revealed that these DEGs were enriched in multiple pathways, including the NF-κB pathway (Figure 5B).

Among the DEGs, COX2, an oxidase reductase, was found to be regulated through the NF-κB pathway. Our results indicated that *COX2* mRNA expression was significantly lower in CD146- MSCs than in CD146+ MSCs on the basis of data from the Gene Expression Omnibus database (Figure 5C). Additionally, COX2 mRNA and protein levels were significantly increased in CD146+ MSCs (Figure 5D and E). CD146-MSCs also exhibited dysregulated p-NF-κB expression, with no significant effect on NF-κB levels (Figure 5E).

As a recognized NF-κB inhibitor, the mechanism of action of CAPE has been confirmed by multiple studies: It specifically inhibits the activity of the IkappaB kinase complex, blocks the phosphorylation and degradation of IkappaBα, and then inhibits the nuclear translocation and transcriptional activation of the NF-κB dimer[34]. Activated NF-κB (P65) needs to enter the nucleus to initiate target gene transcription[35]. CAPE directly inhibits the nuclear transport of p65 by interfering with the interaction between the nuclear localization signal of p65 and importin-α/β, thereby reducing the expression of its downstream genes (such as *COX2*)[36]. CAPE inhibits NF-κB phosphorylation[35,37], prompting us to treat CD146+ MSCs with CAPE and analyze NF-κB phosphorylation levels. The results indicated that CAPE inhibited NF-κB phosphorylation in CD146+ MSCs and reduced COX2 expression (Figure 5F and G). Additionally, the secretion of cytokines from CD146+ MSCs was evaluated, and CAPE was found to partially reverse the changes in cytokine secretion in CD146+ MSCs (Figure 5H).

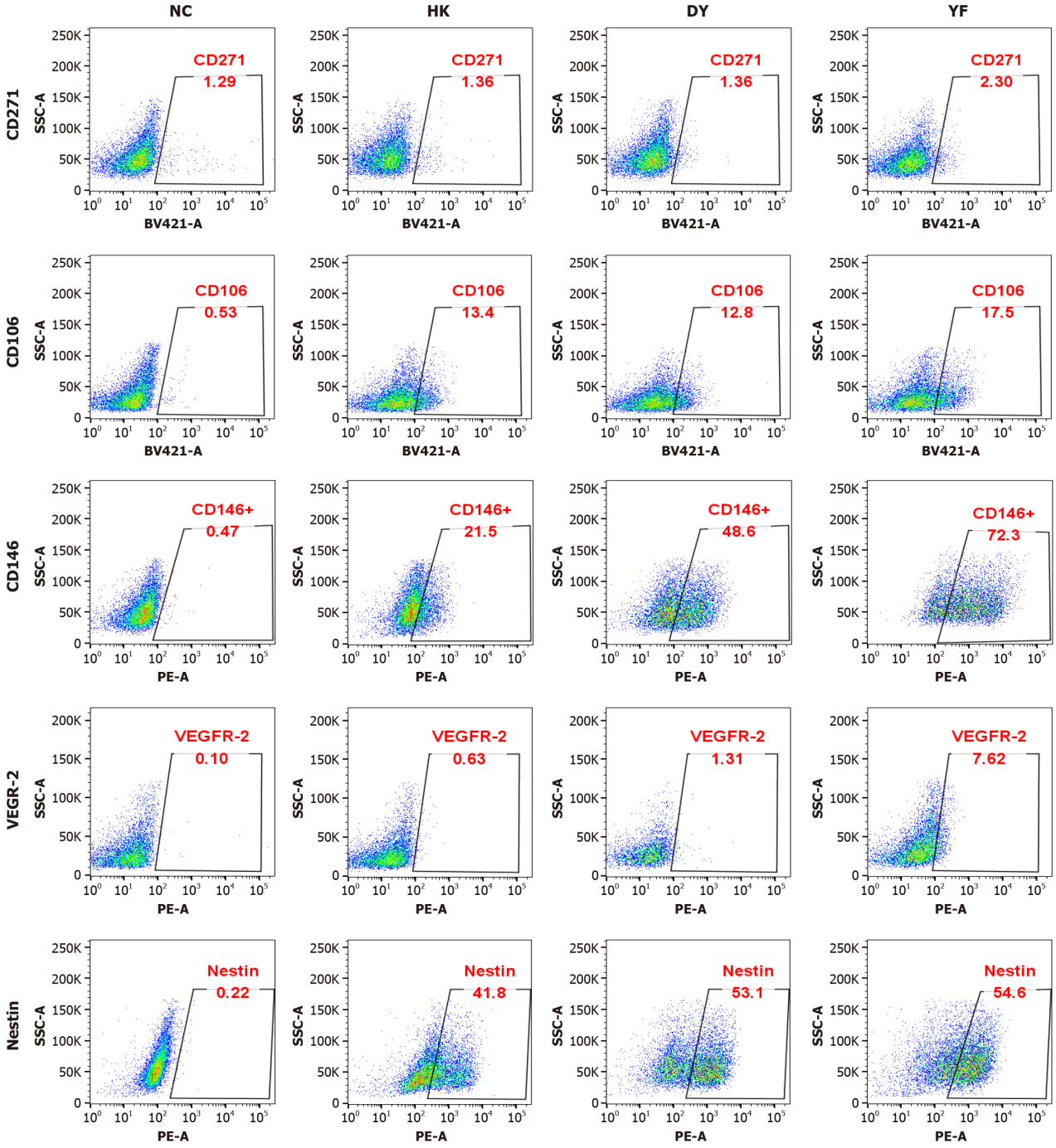

Figure 2 CD146 protein expression in mesenchymal stromal cells cultured in medium from Shandong Qilu Cell Therapy Engineering Technology Co. Ltd., administered *via* caudal vein injection under the acute respiratory distress syndrome model. Variations in the expression of different proteins across various culture systems. Representative flow cytometry patterns from the different groups are shown. The expression of CD146 was significantly greater in the mesenchymal stromal cells cultured in medium from Shandong Qilu Cell Therapy Engineering Technology Co. Ltd., administered *via* caudal vein injection under the acute respiratory distress syndrome model system, whereas the CD271, CD106, vascular endothelial growth factor-2, and Nestin expression levels were not significantly different. NC: Negative control; DY: Mesenchymal stromal cells cultured in medium from Dakewe Biotech Co., administered *via* caudal vein injection after establishing the acute respiratory distress syndrome model; YF: Mesenchymal stromal cells cultured in medium from Shandong Qilu Cell Therapy Engineering Technology Co. Ltd., administered *via* caudal vein injection under the acute respiratory distress syndrome model; HK: Mesenchymal stromal cells cultured in medium from Cytoniche, administered *via* caudal vein injection in the acute respiratory distress syndrome model.

To investigate the mechanism of action of NF-κB in CD146+ MSCs, we found that both the mRNA and protein levels of COX2 were significantly decreased after p65 knockdown (Supplementary Figure 3A and B). We also detected the factors secreted by these cell lines and found that the levels of HGF, PGE2, and VEGF were significantly decreased after p65 knockdown (Supplementary Figure 3C). Taken together, these results indicate that CD146+ MSCs promote COX2 expression by activating the NF-κB pathway. Overall, these findings suggest that CD146+ MSCs upregulate COX2 through the activation of the NF-κB pathway.

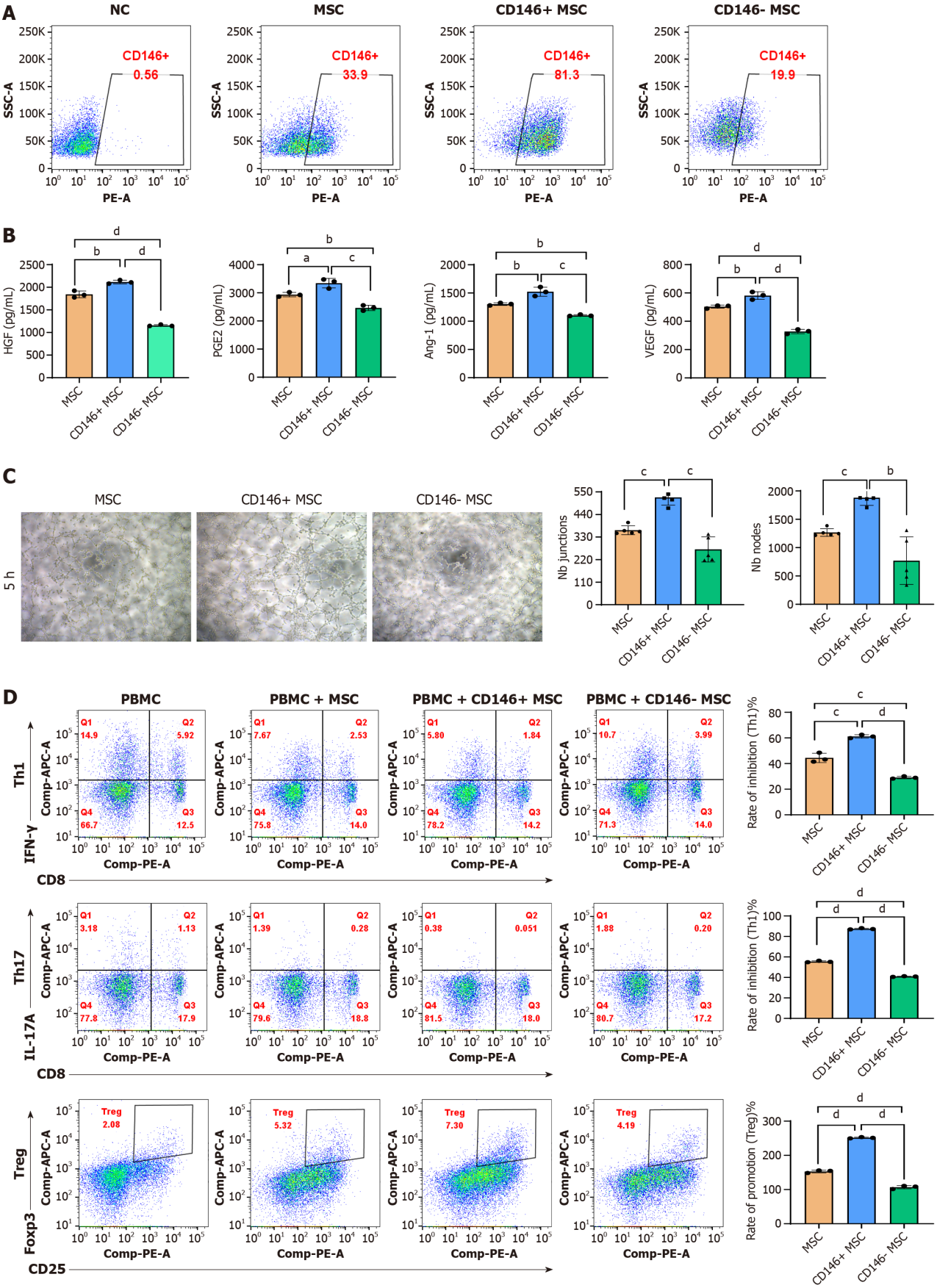

Figure 3 Biological characteristics of the CD146+/- mesenchymal stromal cell subpopulation. A: CD146+ mesenchymal stromal cells (MSCs) and CD146- MSCs were isolated *via* magnetic bead sorting, and the proportion of CD146+ and CD146- MSCs increased from 32.1% to 68.7%; B: Enzyme-linked immunosorbent assay analysis of hepatocyte growth factor, prostaglandin E2, angiopoietin-1, and vascular endothelial growth factor levels in MSCs; C: Human umbilical vein endothelial cells were cultured alone or with either CD146+ MSCs or CD146- MSCs. Cord formation was evaluated at 5 hours post-seeding. Junctions

and nodes were quantified at 5 hours and compared with those in the human umbilical vein endothelial cell-only group; D: *In vitro* immunomodulation by CD146+ MSCs and CD146- MSCs. T helper type 1/T helper type 17/regulatory T cells were cocultured with CD146+ MSCs and CD146- MSCs for 18 hours/3 days. T-cell analysis was performed *via* flow cytometry. The data are presented as the means ± SD and were analyzed *via* two-sided Student's *t* tests. $n = 3$, $^{a}P < 0.05$, $^{b}P < 0.01$, $^{c}P < 0.001$, $^{d}P < 0.0001$. NC: Negative control; MSC: Mesenchymal stromal cell; HGF: Hepatocyte growth factor; PGE2: Prostaglandin E2; Ang-1: Angiopoietin-1; VEGF: Vascular endothelial growth factor; Th1: T helper type 1; Th17: T helper type 17; Treg: Regulatory T; IFN: Interferon; IL: Interleukin.

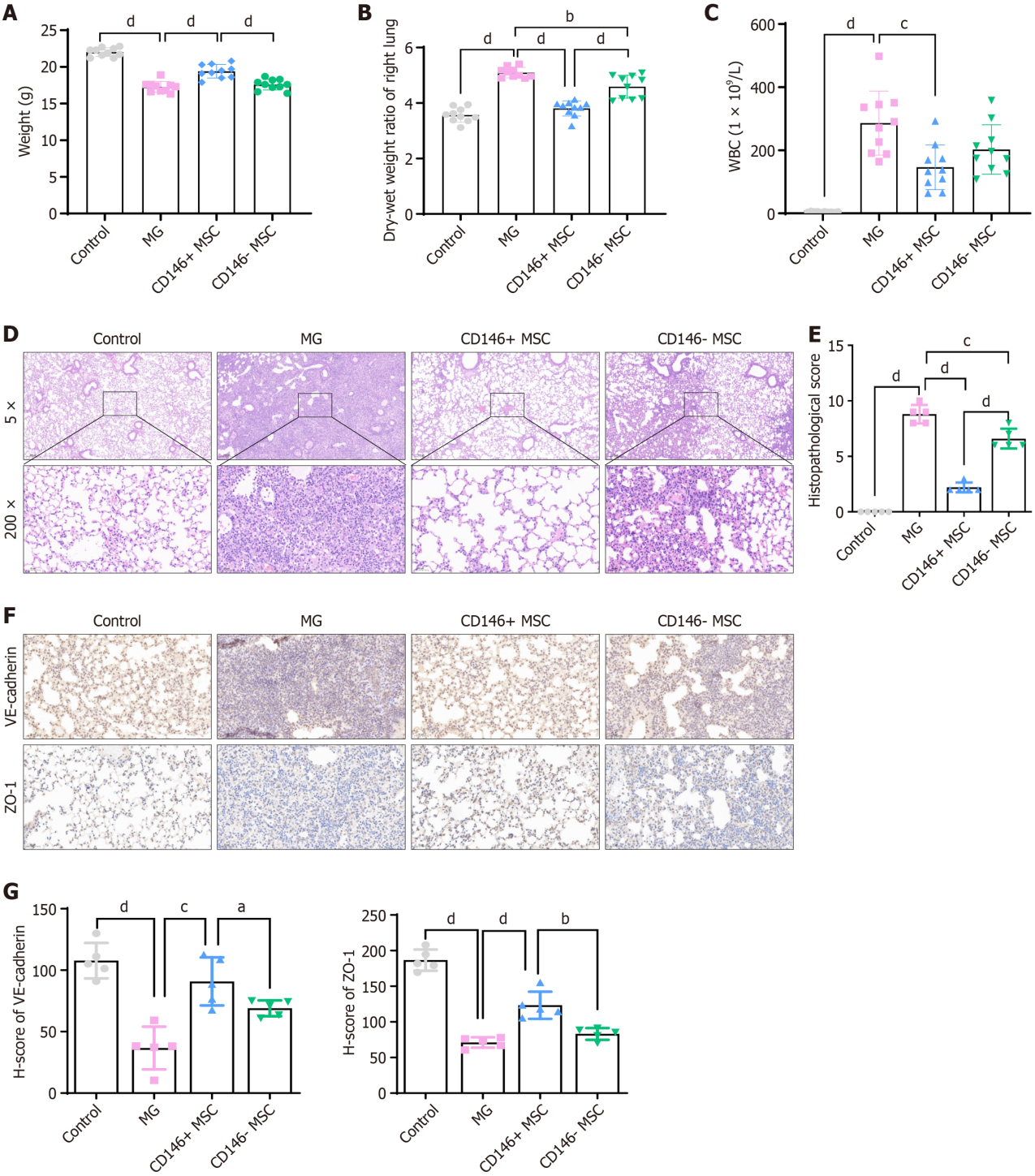

Figure 4 Therapeutic effects on acute respiratory distress syndrome after injection of CD146+ mesenchymal stromal cells and caffeic acid phenethyl ester pretreated CD146+ mesenchymal stromal cells. A and B: Comparison of body weight (A) and wet-dry ratio (B) of lung tissue across groups ($n = 10$ per group); C: White blood cell counts in bronchoalveolar lavage fluid were measured at the experimental endpoint ($n = 10$ per group); D and E: Representative images of pathological changes and lung injury scores (E) in the lung tissue of each group ($n = 5$ per group); F: Representative immunohistochemical images of VE-cadherin and zonula occludens-1 staining in different groups; G: H-scores of VE-cadherin and zonula occludens-1 in mouse lung tissues. The data are

presented as the means ± SD and were analyzed *via* two-sided Student's *t* tests. [a]*P* < 0.05, [b]*P* < 0.01, [c]*P* < 0.001, [d]*P* < 0.0001. WBC: White blood cell; MG: Model control (vehicle administered *via* caudal vein injection after establishing the acute respiratory distress syndrome model; MSC: Mesenchymal stromal cell; ZO-1: Zonula occludens-1.

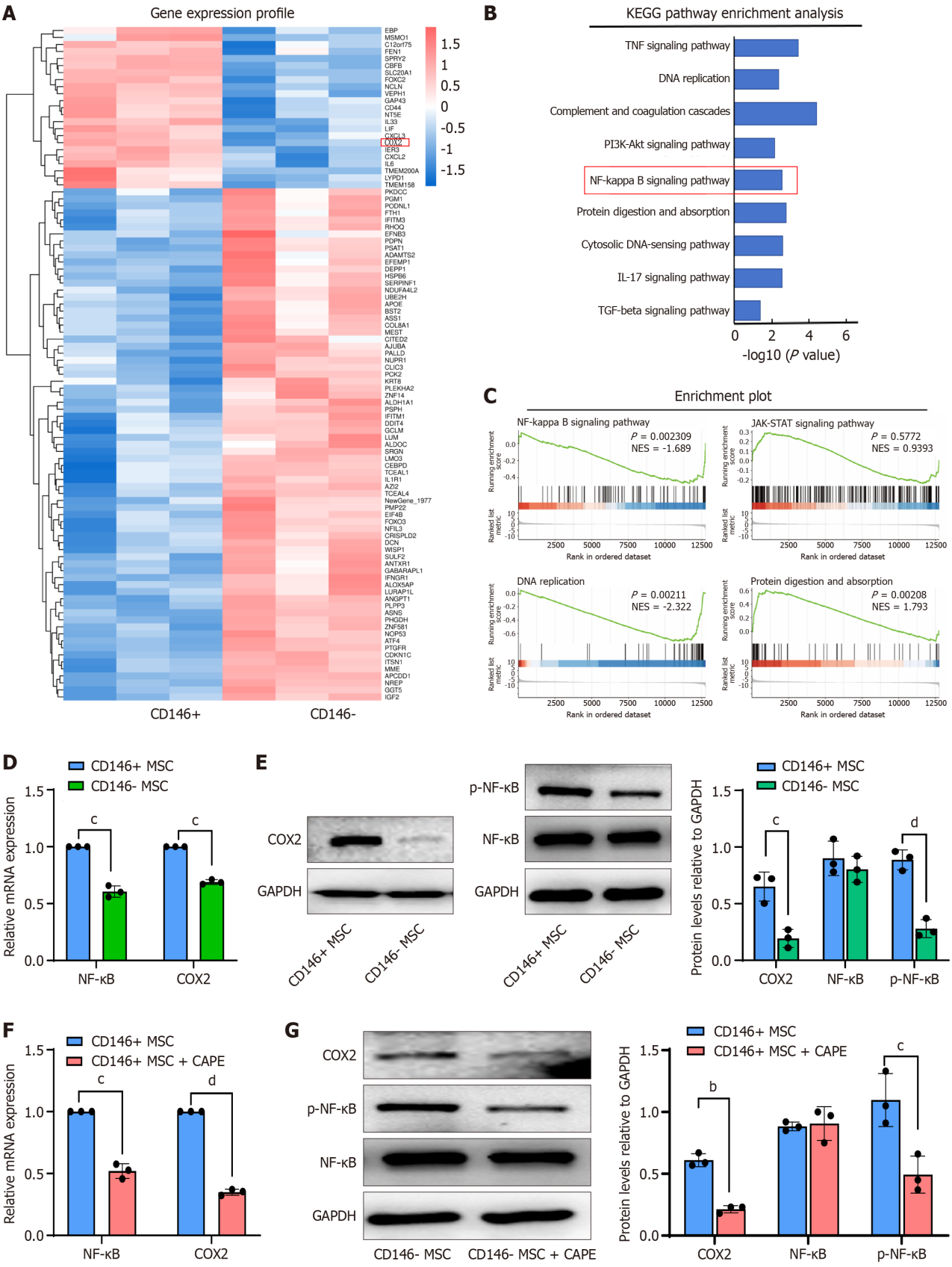

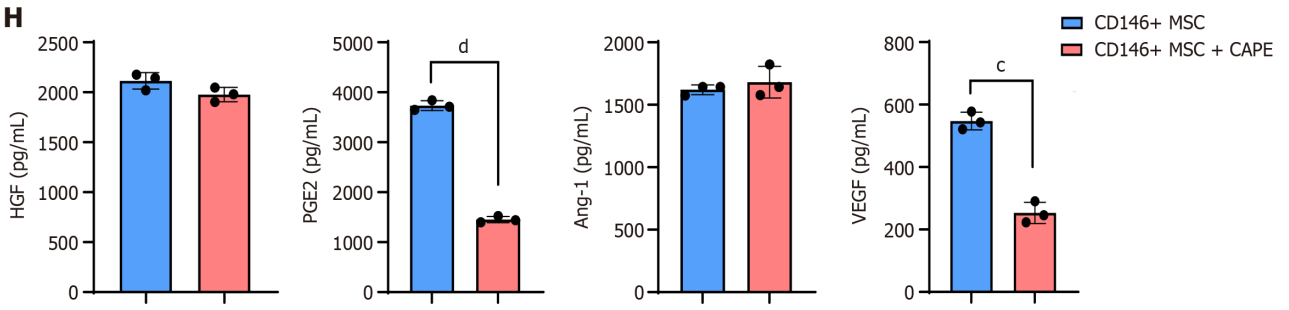

Figure 5 Transcriptomic analysis of mesenchymal stromal cells and validation. A: Heatmap displaying genes differentially expressed between CD146+ mesenchymal stromal cells (MSCs) and CD146- MSCs; B: Kyoto Encyclopedia of Genes and Genomes enrichment analysis demonstrating that differentially expressed genes are enriched in distinct signaling pathways between CD146+ MSCs and CD146- MSCs; C: Gene set enrichment analysis was performed on the differentially expressed genes; D: Cyclooxygenase 2 (*COX2*) and nuclear factor kappa B (*NF-κB*) mRNA levels in CD146+ MSCs and CD146- MSCs were quantified by reverse transcription-quantitative polymerase chain reaction; E: Western blot analysis of COX2, NF-κB, and p-NF-κB protein levels; F: *COX2* and *NF-κB* mRNA levels in CD146+ MSCs treated with caffeic acid phenethyl ester (CAPE) for 24 hours were detected by reverse transcription-quantitative polymerase chain reaction. The band density was compared to that of the control and normalized to that of *GAPDH* using densitometry; G: The protein levels of COX2, NF-κB, and p-NF-κB were detected by western blot in CD146+ MSCs treated with CAPE for 24 hours. Band density was compared to that of the control and normalized to that of GAPDH *via* densitometry; H: Enzyme-linked immunosorbent assay analysis of hepatocyte growth factor, prostaglandin E2, angiopoietin-1, and vascular endothelial growth factor expression in CD146+ MSCs after treatment with CAPE for 24 hours. Data are presented as the means ± SD and were analyzed by two-sided Student's *t* tests. $n = 3$. $^{a}P < 0.05$, $^{b}P < 0.01$, $^{c}P < 0.001$, $^{d}P < 0.0001$. KEGG: Kyoto Encyclopedia of Genes and Genomes; TNF: Tumor necrosis factor; PI3K: Phosphoinositide 3-kinases; IL: Interleukin; TGF: Transforming growth factor; MSC: Mesenchymal stromal cell; NF-κB: Nuclear factor kappa B; COX2: Cyclooxygenase 2; CAPE: Caffeic acid phenethyl ester; HGF: Hepatocyte growth factor; PGE2: Prostaglandin E2; Ang-1: Angiopoietin-1; VEGF: Vascular endothelial growth factor.

CD146+ MSCs significantly reduce LPS-induced damage to human lung microvascular endothelial cells

A cell permeability assay was used to evaluate the effect of MSCs on the barrier function of LPS-induced HULEC-5a cells. Specifically, by detecting the fluorescence intensity of 4 kDa FITC-dextran passing through the transwell membrane, the changes in permeability of the cell monolayer were quantified to verify whether MSCs improve endothelial barrier function by maintaining the integrity of tight junctions. An excessive inflammatory response is a core pathological feature of ARDS that can directly mediate endothelial cell injury, and this assay can verify the immunomodulatory effect of MSCs. Endothelial cell apoptosis assays revealed that CD146+ MSCs support the survival of endothelial cells.

We evaluated permeability, inflammatory factor secretion, and apoptosis in HULEC-5a cells and found that CD146+ MSCs reduced cell damage. Furthermore, CAPE partially restored the effects on HULEC-5a/HPAEpic-II-SV40 permeability, HULEC-5a inflammatory factor secretion, and apoptosis (Figure 6A-D). In addition, p-PKA, p-CREB, VE-cadherin, and ZO-1 Levels were significantly greater in the CD146+ MSC group than in the LPS group, with CAPE partially reversing these effects in CD146+ MSCs (Figure 6E-G). Overall, these results suggest that CD146+ MSCs promote lung epithelial cell repair through the activation of the NF-κB pathway.

DISCUSSION

ARDS is an acute, widespread lung injury caused by various intrapulmonary and extrapulmonary factors that may progress to acute respiratory failure. The primary pathological features include damage to pulmonary vascular endothelial cells, extensive lung inflammation, and osmotic pulmonary edema due to increased pulmonary microvascular permeability[38]. As a result, effectively reducing pulmonary inflammation and protecting endothelial barrier function in the pulmonary microvasculature are crucial approaches to lowering ARDS mortality. Vascular permeability serves as a selective mechanism for maintaining material exchange between blood vessels, tissues, and organs. Disruption of intercellular junctions and the formation of gaps between endothelial cells are key indicators of increased vascular permeability[39]. The functional status of endothelial cells is a major determinant of vascular permeability, and the integrity of endothelial cell junctions is regulated by proteins involved in tight and adherens junctions[38,40,41]. ZO-1 and VE-cadherin are essential components of tight and adherens junctions and are frequently used as indicators for assessing changes in endothelial cell permeability[42].

CD146, a membrane glycoprotein, is highly expressed in various cell types and plays a pivotal role in the activity of vascular endothelial cells and angiogenesis[11,12]. Moreover, CD146 is considered a valuable surface marker for identifying specific MSC subsets[43]. Studies on CD146+ stem cell subsets suggest that CD146 can be used as a quality marker for these MSC populations[44]. In regenerative medicine, the CD146+ MSC subpopulation has demonstrated remarkable biological and therapeutic potential[44,45]. MSCs secrete a variety of growth factors, with HGF and VEGF[46,47] being especially important in regulating vascular endothelial permeability[48,49]. Additionally, inflammatory factors and injury mediators, such as LPS, can induce the production of VEGF and HGF in MSCs[50]. As a result, the paracrine secretion of VEGF and HGF may play a crucial role in regulating vascular permeability during acute lung injury. Moreover, PGE2 alleviates vascular leakage and supports barrier function in human microvascular pulmonary endothelial cells[51,52]. PGE2 also protects against LPS-induced pneumonia in mouse models by decreasing TNF-α

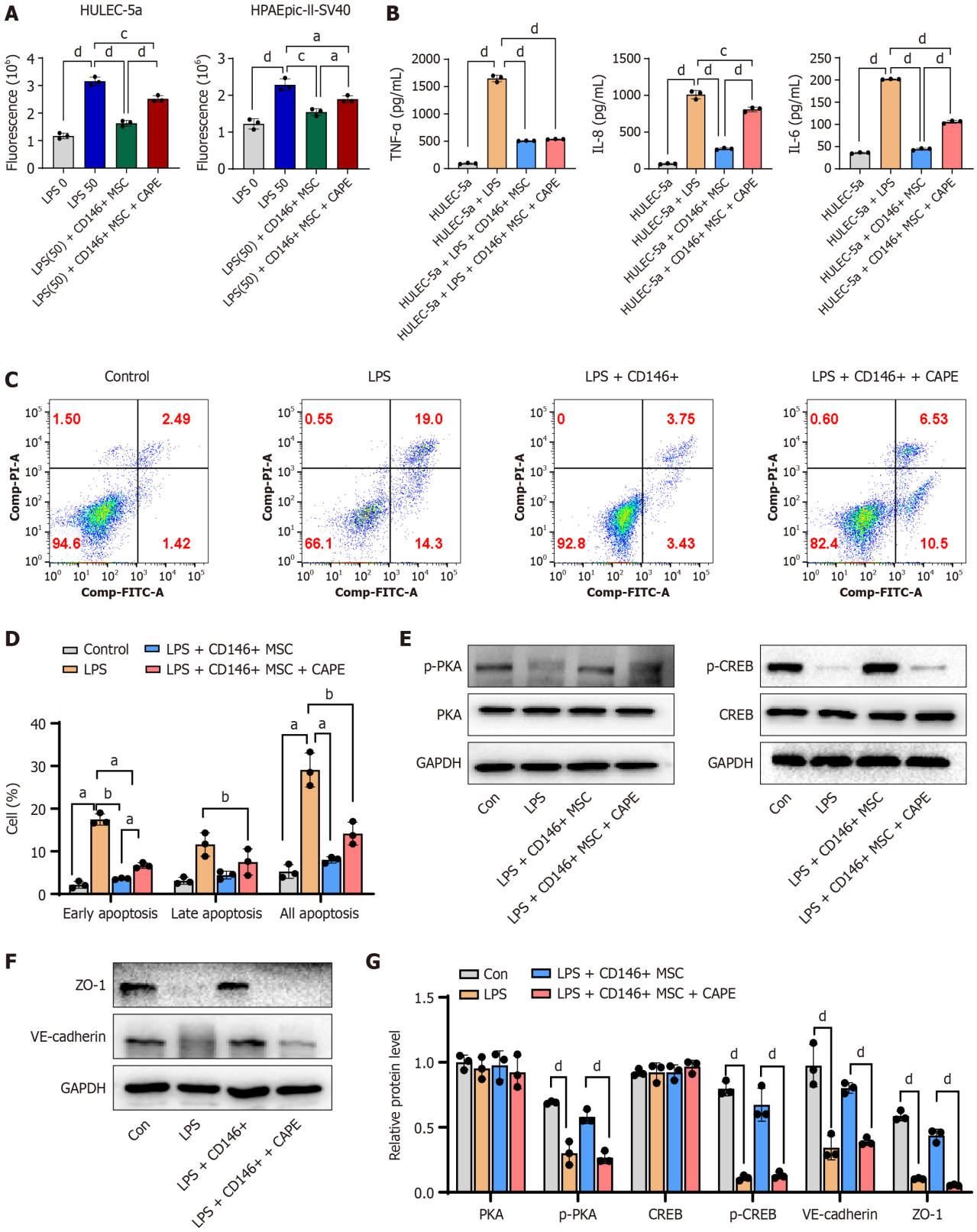

Figure 6 The nuclear factor kappa B inhibitor caffeic acid phenethyl ester reverses the improvement effect of CD146+ mesenchymal stromal cells on pulmonary endothelial barrier injury in acute respiratory distress syndrome. A: Permeability of HULEC-5a/HPAEpic-II-SV40 cells cocultured with CD146+ mesenchymal stromal cells (MSCs) and treated with caffeic acid phenethyl ester for 24 hours; B: The expression of tumor necrosis factor-α, interleukin-8, and interleukin-6 in HULEC-5a cells was measured *via* enzyme-linked immunosorbent assay; C: HULEC-5a cell apoptosis was assessed by Annexin V-FITC and propidium iodide double-staining, followed by flow cytometry analysis after treatment with CD146+ MSCs + caffeic acid phenethyl ester for 24 hours. Representative flow cytometry patterns from different groups are shown; D: Cell apoptosis was measured by Annexin V-APC and propidium iodide double staining and flow cytometric analysis. Representative flow cytometry patterns from different groups are shown. The percentages of apoptotic cells in the different groups were

calculated according to the flow cytometric results; E: Protein levels of protein kinase A, phospho-protein kinase A, cyclic-AMP response element-binding protein, phospho-cyclic-AMP response element-binding protein; F: Western blot analysis of zonula occludens-1, VE-cadherin, and GAPDH protein expression in HULVE-a cells after lipopolysaccharide (LPS)-induced modeling (24 hours) and different treatments; G: The density of each individual band was compared to that of the corresponding control band and normalized to that of GAPDH by densitometry. Groups: Control, LPS, LPS + CD146+ MSC, and LPS + CD146+ MSC + caffeic acid phenethyl ester. The data are presented as the mean ± SD and were analyzed by two-sided Student's *t* tests. $n = 3$. $^{a}P < 0.05$, $^{b}P < 0.01$, $^{c}P < 0.001$, $^{d}P < 0.0001$. LPS: Lipopolysaccharide; TNF: Tumor necrosis factor; IL: Interleukin; CAPE: Caffeic acid phenethyl ester; MSC: Mesenchymal stromal cell; PKA: Protein kinase A; CREB: Cyclic-AMP response element-binding protein; ZO-1: Zonula occludens-1.

secretion and neutrophil recruitment[53]. However, the mechanisms underlying the enhanced functionality of CD146+ MSCs remain unclear.

In this study, we unexpectedly discovered that MSCs cultured in different media significantly differed in their ability to treat ARDS mice and that the YF group presented a greater advantage. Moreover, the expression of MSC CD146 in the YF group was significantly greater than that in the other groups and that CD146+ MSCs could regulate the expression of COX2. Therefore, we hypothesize that there is a potential signaling axis, the CD146/NF-κB/COX2 axis, in CD146+ MSCs. Activation of the NF-κB pathway and upregulation of COX2 contribute to the repair of damaged epithelial cells. Moreover, we observed enhanced pro-angiogenic and anti-inflammatory autocrine factor production: CD146+ MSCs expressed increased levels of HGF, PGE2, VEGF, and Ang-1, contributing to a stronger pro-angiogenic effect and anti-inflammatory effect.

COX, a key enzyme in arachidonic acid metabolism, has two isoforms: COX-1 and COX-2. COX-2 is an inducible enzyme not found under normal physiological conditions but is upregulated during inflammation and tumorigenesis. COX-2 expression is expressed in various inflammatory and traumatic diseases, as well as in multiple tumor types[54-57], and plays a significant role in the progression of osteoarthritis, particularly in cartilage inflammation and joint destruction. COX-2 has been implicated in both the initiation and resolution phases of inflammation, where it initiates the inflammatory response at the early stages and helps resolve inflammation during the recovery phase. PGE2, produced from arachidonic acid by COX-2, is involved in regulating blood pressure and protecting the gastrointestinal mucosa under normal conditions. Additionally, PGE2 acts as an immunosuppressive mediator, inhibiting pro-inflammatory factors in monocytes and promoting IL-10 expression. VEGF, a potent stimulator of osteogenesis, is crucial for the coupling of osteogenesis and angiogenesis[58]. COX-2, a rate-limiting enzyme in prostaglandin synthesis, is expressed under inflammatory, tumorigenic, and hypoxic conditions[59]. COX-2 activation increases the production of both PGE2 and VEGF *in vitro*, whereas inhibiting COX-2 reduces VEGF expression *in vivo*[60]. Moreover, MSC-derived conditioned media has been shown to support endothelial cell growth, promote tube formation, and reduce cell apoptosis, largely through the action of VEGF[61]. MSCs improve pulmonary endothelial barrier injury in ARDS through various pathways, including maintaining barrier integrity, inhibiting excessive inflammatory responses, and reducing endothelial cell apoptosis. Therefore, we designed three *in vitro* experiments to verify the therapeutic mechanisms of CD146+ MSCs from different pathological links.

Pulmonary endothelial cell permeability assay: This assay quantified the reparative effect of MSCs on LPS-induced endothelial barrier disruption. An excessive inflammatory response is a core pathological feature of ARDS that directly mediates endothelial cell injury. This study verified the immunomodulatory effect of CD146+ MSCs. Endothelial cell apoptosis assays clarified the support of CD146+ MSCs for the survival of endothelial cells. Together, these three experiments constitute a complete logical chain of "preventing injury/repairing structure/maintaining function", demonstrating that CD146+ MSCs have sufficient advantages in improving pulmonary endothelial barrier injury in ARDS. These observations were confirmed in an *in vitro* model.

In summary, we found that, compared with CD146- MSCs, CD146+ MSCs demonstrated superior immunomodulatory abilities and cytokine secretion. This may be attributed to the activation of the NF-κB pathway and increased COX2 expression. Therefore, CD146 expression plays a pivotal role in influencing the stem cell properties of MSCs, likely contributing to the enhancement of MSC-mediated regulatory mechanisms.

CONCLUSION

This study demonstrated that, compared with CD146- MSCs, CD146- MSCs exhibit superior therapeutic efficacy in ARDS, primarily due to their increased secretory capacity and immunomodulatory properties. Specifically, CD146+ MSCs effectively promoted alveolar vascular regeneration and mitigated excessive inflammatory responses, which are crucial for lung tissue repair, in ARDS models. Mechanistically, the activation of the NF-κB/COX2 signaling pathway was identified as a key molecular event underlying the epithelial reparative functions of CD146+ MSCs; this pathway regulated the secretion of PGE2 and angiogenic factors, thereby facilitating alveolar epithelial cell proliferation and barrier restoration. These findings not only reveal the subtype-specific functional divergence in MSCs and highlight CD146 as a pivotal marker for isolating MSCs with enhanced therapeutic potential but also establish CD146+ MSCs as a promising cell subtype for targeted ARDS therapy. Moreover, the identification of the NF-κB/COX2 axis as a regulatory hub for MSC-mediated repair provides novel insights into the molecular mechanisms governing MSC heterogeneity, potentially informing the development of precision cell therapies and pharmacologic strategies to optimize therapeutic outcomes in ARDS and other inflammatory diseases.

FOOTNOTES

Author contributions: Tan Y and Ma HR conceived of and designed the study, supervised the research, and revised the manuscript critically for intellectual content; they contributed equally to this manuscript and are co-corresponding authors; Zhang YL designed the experiments; Zhang YL, Wen DK, and Wang SN performed the experiments; Zhang YL and Wang SN analyzed the data; Zhang YL drafted the manuscript. All authors read and approved the final manuscript.

Supported by the Science and Technology SMEs Innovation Capacity Improvement Project of Shandong Province, No. 2022TSGC1004; and National Key R&D Program of China, No. 2021YFA1101502.

Institutional review board statement: The source, screening, and collection process of human umbilical cords at Yantai Yuhuangding Hospital Affiliated with Qingdao University met the national ethical requirements, and the ethical approval number was[2021]003.

Institutional animal care and use committee statement: All procedures involving animals were reviewed and approved by the Institutional Animal Care and Use Committee of the Experimental Animal Ethics Committee of Army Medical University approved the experiments, and the ethical approval number was No. AMUWEC20210830.

Conflict-of-interest statement: All the authors report no relevant conflicts of interest for this article.

Data sharing statement: The datasets generated during and/or analyzed during the current study are available from the corresponding author on reasonable request.

ARRIVE guidelines statement: The authors have read the ARRIVE guidelines, and the manuscript was prepared and revised according to the ARRIVE guidelines.

Country of origin: China

ORCID number: He-Ran Ma 0000-0003-1981-4947.

S-Editor: Wang JJ
L-Editor: Filipodia
P-Editor: Wang CH

REFERENCES

1 **Han Y**, Li X, Zhang Y, Han Y, Chang F, Ding J. Mesenchymal Stem Cells for Regenerative Medicine. *Cells* 2019; **8**: 886 [*RCA*] [PMID: 31412678 DOI: 10.3390/cells8080886] [FullText] [Full Text(PDF)]
2 **Van Nguyen TT**, Vu NB, Van Pham P. Mesenchymal Stem Cell Transplantation for Ischemic Diseases: Mechanisms and Challenges. *Tissue Eng Regen Med* 2021; **18**: 587-611 [*RCA*] [PMID: 33884577 DOI: 10.1007/s13770-021-00334-3] [FullText]
3 **Burnham AJ**, Daley-Bauer LP, Horwitz EM. Mesenchymal stromal cells in hematopoietic cell transplantation. *Blood Adv* 2020; **4**: 5877-5887 [*RCA*] [PMID: 33232479 DOI: 10.1182/bloodadvances.2020002646] [FullText]
4 **Zheng W**, Li H, Hu K, Li L, Bei M. Chondromalacia patellae: current options and emerging cell therapies. *Stem Cell Res Ther* 2021; **12**: 412 [*RCA*] [PMID: 34275494 DOI: 10.1186/s13287-021-02478-4] [FullText] [Full Text(PDF)]
5 **Dominici M**, Le Blanc K, Mueller I, Slaper-Cortenbach I, Marini F, Krause D, Deans R, Keating A, Prockop Dj, Horwitz E. Minimal criteria for defining multipotent mesenchymal stromal cells. The International Society for Cellular Therapy position statement. *Cytotherapy* 2006; **8**: 315-317 [*RCA*] [PMID: 16923606 DOI: 10.1080/14653240600855905] [FullText]
6 **Costa LA**, Eiro N, Fraile M, Gonzalez LO, Saá J, Garcia-Portabella P, Vega B, Schneider J, Vizoso FJ. Functional heterogeneity of mesenchymal stem cells from natural niches to culture conditions: implications for further clinical uses. *Cell Mol Life Sci* 2021; **78**: 447-467 [*RCA*] [PMID: 32699947 DOI: 10.1007/s00018-020-03600-0] [FullText] [Full Text(PDF)]
7 **Lv FJ**, Tuan RS, Cheung KM, Leung VY. Concise review: the surface markers and identity of human mesenchymal stem cells. *Stem Cells* 2014; **32**: 1408-1419 [*RCA*] [PMID: 24578244 DOI: 10.1002/stem.1681] [FullText]
8 **Bikorimana JP**, Saad W, Abusarah J, Lahrichi M, Talbot S, Shammaa R, Rafei M. CD146 Defines a Mesenchymal Stromal Cell Subpopulation with Enhanced Suppressive Properties. *Cells* 2022; **11**: 2263 [*RCA*] [PMID: 35892560 DOI: 10.3390/cells11152263] [FullText] [Full Text(PDF)]
9 **Lehmann JM**, Holzmann B, Breitbart EW, Schmiegelow P, Riethmüller G, Johnson JP. Discrimination between benign and malignant cells of melanocytic lineage by two novel antigens, a glycoprotein with a molecular weight of 113,000 and a protein with a molecular weight of 76,000. *Cancer Res* 1987; **47**: 841-845 [*RCA*] [PMID: 3542195] [FullText]
10 **Lehmann JM**, Riethmüller G, Johnson JP. MUC18, a marker of tumor progression in human melanoma, shows sequence similarity to the neural cell adhesion molecules of the immunoglobulin superfamily. *Proc Natl Acad Sci U S A* 1989; **86**: 9891-9895 [*RCA*] [PMID: 2602381 DOI: 10.1073/pnas.86.24.9891] [FullText]
11 **Lerman DA**, Diaz M, Peault B. Changes in coexpression of pericytes and endogenous cardiac progenitor cells from heart development to

disease state. *Eur Heart J* 2018; **39**: P1850 [*RCA*] [PMID: 30270958 DOI: 10.1093/eurheartj/ehy565.P1850] [FullText]

12 **Chen J**, Luo Y, Hui H, Cai T, Huang H, Yang F, Feng J, Zhang J, Yan X. CD146 coordinates brain endothelial cell-pericyte communication for blood-brain barrier development. *Proc Natl Acad Sci U S A* 2017; **114**: E7622-E7631 [*RCA*] [PMID: 28827364 DOI: 10.1073/pnas.1710848114] [FullText] [Full Text(PDF)]

13 **Wang Z**, Yan X. CD146, a multi-functional molecule beyond adhesion. *Cancer Lett* 2013; **330**: 150-162 [*RCA*] [PMID: 23266426 DOI: 10.1016/j.canlet.2012.11.049] [FullText]

14 **Wu CC**, Liu FL, Sytwu HK, Tsai CY, Chang DM. CD146+ mesenchymal stem cells display greater therapeutic potential than CD146- cells for treating collagen-induced arthritis in mice. *Stem Cell Res Ther* 2016; **7**: 23 [*RCA*] [PMID: 26841872 DOI: 10.1186/s13287-016-0285-4] [Full Text] [Full Text(PDF)]

15 **Harkness L**, Zaher W, Ditzel N, Isa A, Kassem M. CD146/MCAM defines functionality of human bone marrow stromal stem cell populations. *Stem Cell Res Ther* 2016; **7**: 4 [*RCA*] [PMID: 26753846 DOI: 10.1186/s13287-015-0266-z] [FullText] [Full Text(PDF)]

16 **Wangler S**, Menzel U, Li Z, Ma J, Hoppe S, Benneker LM, Alini M, Grad S, Peroglio M. CD146/MCAM distinguishes stem cell subpopulations with distinct migration and regenerative potential in degenerative intervertebral discs. *Osteoarthritis Cartilage* 2019; **27**: 1094-1105 [*RCA*] [PMID: 31002939 DOI: 10.1016/j.joca.2019.04.002] [FullText]

17 **Bowles AC**, Kouroupis D, Willman MA, Perucca Orfei C, Agarwal A, Correa D. Signature quality attributes of CD146(+) mesenchymal stem/stromal cells correlate with high therapeutic and secretory potency. *Stem Cells* 2020; **38**: 1034-1049 [*RCA*] [PMID: 32379908 DOI: 10.1002/stem.3196] [FullText]

18 **Lee NE**, Kim SJ, Yang SJ, Joo SY, Park H, Lee KW, Yang HM, Park JB. Comparative characterization of mesenchymal stromal cells from multiple abdominal adipose tissues and enrichment of angiogenic ability *via* CD146 molecule. *Cytotherapy* 2017; **19**: 170-180 [*RCA*] [PMID: 28024875 DOI: 10.1016/j.jcyt.2016.11.002] [FullText]

19 **Lauvrud AT**, Kelk P, Wiberg M, Kingham PJ. Characterization of human adipose tissue-derived stem cells with enhanced angiogenic and adipogenic properties. *J Tissue Eng Regen Med* 2017; **11**: 2490-2502 [*RCA*] [PMID: 26833948 DOI: 10.1002/term.2147] [FullText]

20 **Gomes JP**, Coatti GC, Valadares MC, Assoni AF, Pelatti MV, Secco M, Zatz M. Human Adipose-Derived CD146(+) Stem Cells Increase Life Span of a Muscular Dystrophy Mouse Model More Efficiently than Mesenchymal Stromal Cells. *DNA Cell Biol* 2018; **37**: 798-804 [*RCA*] [PMID: 30059260 DOI: 10.1089/dna.2018.4158] [FullText]

21 **Ulrich C**, Abruzzese T, Maerz JK, Ruh M, Amend B, Benz K, Rolauffs B, Abele H, Hart ML, Aicher WK. Human Placenta-Derived CD146-Positive Mesenchymal Stromal Cells Display a Distinct Osteogenic Differentiation Potential. *Stem Cells Dev* 2015; **24**: 1558-1569 [*RCA*] [PMID: 25743703 DOI: 10.1089/scd.2014.0465] [FullText]

22 **Wu YX**, Jing XZ, Sun Y, Ye YP, Guo JC, Huang JM, Xiang W, Zhang JM, Guo FJ. CD146+ skeletal stem cells from growth plate exhibit specific chondrogenic differentiation capacity in vitro. *Mol Med Rep* 2017; **16**: 8019-8028 [*RCA*] [PMID: 28983600 DOI: 10.3892/mmr.2017.7616] [FullText] [Full Text(PDF)]

23 **Allen RJ**, Guillen-Guio B, Oldham JM, Ma SF, Dressen A, Paynton ML, Kraven LM, Obeidat M, Li X, Ng M, Braybrooke R, Molina-Molina M, Hobbs BD, Putman RK, Sakornsakolpat P, Booth HL, Fahy WA, Hart SP, Hill MR, Hirani N, Hubbard RB, McAnulty RJ, Millar AB, Navaratnam V, Oballa E, Parfrey H, Saini G, Whyte MKB, Zhang Y, Kaminski N, Adegunsoye A, Strek ME, Neighbors M, Sheng XR, Gudmundsson G, Gudnason V, Hatabu H, Lederer DJ, Manichaikul A, Newell JD Jr, O'Connor GT, Ortega VE, Xu H, Fingerlin TE, Bossé Y, Hao K, Joubert P, Nickle DC, Sin DD, Timens W, Furniss D, Morris AP, Zondervan KT, Hall IP, Sayers I, Tobin MD, Maher TM, Cho MH, Hunninghake GM, Schwartz DA, Yaspan BL, Molyneaux PL, Flores C, Noth I, Jenkins RG, Wain LV. Genome-Wide Association Study of Susceptibility to Idiopathic Pulmonary Fibrosis. *Am J Respir Crit Care Med* 2020; **201**: 564-574 [*RCA*] [PMID: 31710517 DOI: 10.1164/rccm.201905-1017OC] [FullText] [Full Text(PDF)]

24 **Silva JD**, Krasnodembskaya AD. Investigation of the MSC Paracrine Effects on Alveolar-Capillary Barrier Integrity in the In Vitro Models of ARDS. *Methods Mol Biol* 2021; **2269**: 63-81 [*RCA*] [PMID: 33687672 DOI: 10.1007/978-1-0716-1225-5_5] [FullText]

25 **Dutra Silva J**, Su Y, Calfee CS, Delucchi KL, Weiss D, McAuley DF, O'Kane C, Krasnodembskaya AD. Mesenchymal stromal cell extracellular vesicles rescue mitochondrial dysfunction and improve barrier integrity in clinically relevant models of ARDS. *Eur Respir J* 2021; **58**: 2002978 [*RCA*] [PMID: 33334945 DOI: 10.1183/13993003.02978-2020] [FullText] [Full Text(PDF)]

26 **Natarajan K**, Singh S, Burke TR Jr, Grunberger D, Aggarwal BB. Caffeic acid phenethyl ester is a potent and specific inhibitor of activation of nuclear transcription factor NF-kappa B. *Proc Natl Acad Sci U S A* 1996; **93**: 9090-9095 [*RCA*] [PMID: 8799159 DOI: 10.1073/pnas.93.17.9090] [FullText]

27 **Onori P**, DeMorrow S, Gaudio E, Franchitto A, Mancinelli R, Venter J, Kopriva S, Ueno Y, Alvaro D, Savage J, Alpini G, Francis H. Caffeic acid phenethyl ester decreases cholangiocarcinoma growth by inhibition of NF-kappaB and induction of apoptosis. *Int J Cancer* 2009; **125**: 565-576 [*RCA*] [PMID: 19358267 DOI: 10.1002/ijc.24271] [FullText] [Full Text(PDF)]

28 **D'Alessio FR**. Mouse Models of Acute Lung Injury and ARDS. *Methods Mol Biol* 2018; **1809**: 341-350 [*RCA*] [PMID: 29987799 DOI: 10.1007/978-1-4939-8570-8_22] [FullText]

29 **Chen R**, Xie F, Zhao J, Yue B. Suppressed nuclear factor-kappa B alleviates lipopolysaccharide-induced acute lung injury through downregulation of CXCR4 mediated by microRNA-194. *Respir Res* 2020; **21**: 144 [*RCA*] [PMID: 32522221 DOI: 10.1186/s12931-020-01391-3] [FullText] [Full Text(PDF)]

30 **Zhang Y**, Ma Y, Wu G, Xie M, Luo C, Huang X, Tian F, Chen J, Li X. SENP1 promotes MCL pathogenesis through regulating JAK-STAT5 pathway and SOCS2 expression. *Cell Death Discov* 2021; **7**: 192 [*RCA*] [PMID: 34312374 DOI: 10.1038/s41420-021-00578-x] [FullText] [Full Text(PDF)]

31 **Galipeau J**, Krampera M, Barrett J, Dazzi F, Deans RJ, DeBruijn J, Dominici M, Fibbe WE, Gee AP, Gimble JM, Hematti P, Koh MB, LeBlanc K, Martin I, McNiece IK, Mendicino M, Oh S, Ortiz L, Phinney DG, Planat V, Shi Y, Stroncek DF, Viswanathan S, Weiss DJ, Sensebe L. International Society for Cellular Therapy perspective on immune functional assays for mesenchymal stromal cells as potency release criterion for advanced phase clinical trials. *Cytotherapy* 2016; **18**: 151-159 [*RCA*] [PMID: 26724220 DOI: 10.1016/j.jcyt.2015.11.008] [FullText]

32 **Rozenberg A**, Rezk A, Boivin MN, Darlington PJ, Nyirenda M, Li R, Jalili F, Winer R, Artsy EA, Uccelli A, Reese JS, Planchon SM, Cohen JA, Bar-Or A. Human Mesenchymal Stem Cells Impact Th17 and Th1 Responses Through a Prostaglandin E2 and Myeloid-Dependent Mechanism. *Stem Cells Transl Med* 2016; **5**: 1506-1514 [*RCA*] [PMID: 27400792 DOI: 10.5966/sctm.2015-0243] [FullText] [Full Text(PDF)]

33 **Heidari M**, Pouya S, Baghaei K, Aghdaei HA, Namaki S, Zali MR, Hashemi SM. The immunomodulatory effects of adipose-derived mesenchymal stem cells and mesenchymal stem cells-conditioned medium in chronic colitis. *J Cell Physiol* 2018; **233**: 8754-8766 [*RCA*]

[PMID: 29797577 DOI: 10.1002/jcp.26765] [FullText]

34 **Darwish SS**, Chen PJ, Hamed MM, Wagdy RA, Chen SH, Abadi AH, Abdel-Halim M, Hwang TL, Engel M. Development of (4-Phenylamino)quinazoline Alkylthiourea Derivatives as Novel NF-κB Inhibitors. *Pharmaceuticals (Basel)* 2022; **15**: 778 [*RCA*] [PMID: 35890077 DOI: 10.3390/ph15070778] [FullText] [Full Text(PDF)]

35 **Liu Q**, Du J, Yu X, Xu J, Huang F, Li X, Zhang C, Li X, Chang J, Shang D, Zhao Y, Tian M, Lu H, Xu J, Li C, Zhu H, Jin N, Jiang C. miRNA-200c-3p is crucial in acute respiratory distress syndrome. *Cell Discov* 2017; **3**: 17021 [*RCA*] [PMID: 28690868 DOI: 10.1038/celldisc.2017.21] [FullText] [Full Text(PDF)]

36 **Kuo HC**, Kuo WH, Lee YJ, Wang CJ, Tseng TH. Enhancement of caffeic acid phenethyl ester on all-trans retinoic acid-induced differentiation in human leukemia HL-60 cells. *Toxicol Appl Pharmacol* 2006; **216**: 80-88 [*RCA*] [PMID: 16766008 DOI: 10.1016/j.taap.2006.04.007] [Full Text]

37 **Kuang L**, Wu J, Su N, Qi H, Chen H, Zhou S, Xiong Y, Du X, Tan Q, Yang J, Jin M, Luo F, Ouyang J, Zhang B, Wang Z, Jiang W, Chen L, Chen S, Wang Z, Liu P, Yin L, Guo F, Deng C, Chen D, Liu C, Xie Y, Ni Z, Chen L. FGFR3 deficiency enhances CXCL12-dependent chemotaxis of macrophages *via* upregulating CXCR7 and aggravates joint destruction in mice. *Ann Rheum Dis* 2020; **79**: 112-122 [*RCA*] [PMID: 31662319 DOI: 10.1136/annrheumdis-2019-215696] [FullText]

38 **Jiang J**, Huang K, Xu S, Garcia JGN, Wang C, Cai H. Targeting NOX4 alleviates sepsis-induced acute lung injury *via* attenuation of redox-sensitive activation of CaMKII/ERK1/2/MLCK and endothelial cell barrier dysfunction. *Redox Biol* 2020; **36**: 101638 [*RCA*] [PMID: 32863203 DOI: 10.1016/j.redox.2020.101638] [FullText] [Full Text(PDF)]

39 **Adil MS**, Somanath PR. Endothelial Permeability Assays In Vitro. *Methods Mol Biol* 2021; **2367**: 177-191 [*RCA*] [PMID: 32691355 DOI: 10.1007/7651_2020_309] [FullText]

40 **Yu WK**, McNeil JB, Wickersham NE, Shaver CM, Bastarache JA, Ware LB. Vascular endothelial cadherin shedding is more severe in sepsis patients with severe acute kidney injury. *Crit Care* 2019; **23**: 18 [*RCA*] [PMID: 30658667 DOI: 10.1186/s13054-019-2315-y] [FullText] [Full Text(PDF)]

41 **Li L**, Liu Q, Shang T, Song W, Xu D, Allen TD, Wang X, Jeong J, Lobe CG, Liu J. Aberrant Activation of Notch1 Signaling in Glomerular Endothelium Induces Albuminuria. *Circ Res* 2021; **128**: 602-618 [*RCA*] [PMID: 33435713 DOI: 10.1161/CIRCRESAHA.120.316970] [Full Text]

42 **Wang T**, Liu C, Pan LH, Liu Z, Li CL, Lin JY, He Y, Xiao JY, Wu S, Qin Y, Li Z, Lin F. Inhibition of p38 MAPK Mitigates Lung Ischemia Reperfusion Injury by Reducing Blood-Air Barrier Hyperpermeability. *Front Pharmacol* 2020; **11**: 569251 [*RCA*] [PMID: 33362540 DOI: 10.3389/fphar.2020.569251] [FullText] [Full Text(PDF)]

43 **Covas DT**, Panepucci RA, Fontes AM, Silva WA Jr, Orellana MD, Freitas MC, Neder L, Santos AR, Peres LC, Jamur MC, Zago MA. Multipotent mesenchymal stromal cells obtained from diverse human tissues share functional properties and gene-expression profile with CD146+ perivascular cells and fibroblasts. *Exp Hematol* 2008; **36**: 642-654 [*RCA*] [PMID: 18295964 DOI: 10.1016/j.exphem.2007.12.015] [FullText]

44 **Jin HJ**, Kwon JH, Kim M, Bae YK, Choi SJ, Oh W, Yang YS, Jeon HB. Downregulation of Melanoma Cell Adhesion Molecule (MCAM/CD146) Accelerates Cellular Senescence in Human Umbilical Cord Blood-Derived Mesenchymal Stem Cells. *Stem Cells Transl Med* 2016; **5**: 427-439 [*RCA*] [PMID: 26941359 DOI: 10.5966/sctm.2015-0109] [FullText]

45 **Pavlidis P**, Tsakmaki A, Pantazi E, Li K, Cozzetto D, Digby-Bell J, Yang F, Lo JW, Alberts E, Sa ACC, Niazi U, Friedman J, Long AK, Ding Y, Carey CD, Lamb C, Saqi M, Madgwick M, Gul L, Treveil A, Korcsmaros T, Macdonald TT, Lord GM, Bewick G, Powell N. Interleukin-22 regulates neutrophil recruitment in ulcerative colitis and is associated with resistance to ustekinumab therapy. *Nat Commun* 2022; **13**: 5820 [*RCA*] [PMID: 36192482 DOI: 10.1038/s41467-022-33331-8] [FullText] [Full Text(PDF)]

46 **Crisostomo PR**, Wang Y, Markel TA, Wang M, Lahm T, Meldrum DR. Human mesenchymal stem cells stimulated by TNF-alpha, LPS, or hypoxia produce growth factors by an NF kappa B- but not JNK-dependent mechanism. *Am J Physiol Cell Physiol* 2008; **294**: C675-C682 [*RCA*] [PMID: 18234850 DOI: 10.1152/ajpcell.00437.2007] [FullText]

47 **Kinnaird T**, Stabile E, Burnett MS, Shou M, Lee CW, Barr S, Fuchs S, Epstein SE. Local delivery of marrow-derived stromal cells augments collateral perfusion through paracrine mechanisms. *Circulation* 2004; **109**: 1543-1549 [*RCA*] [PMID: 15023891 DOI: 10.1161/01.CIR.0000124062.31102.57] [FullText]

48 **Liu XL**, Sato S, Dai W, Yamanaka N. The protective effect of hepatocyte growth-promoting factor (pHGF) against hydrogen peroxide-induced acute lung injury in rats. *Med Electron Microsc* 2001; **34**: 92-102 [*RCA*] [PMID: 11685658 DOI: 10.1007/s007950170003] [FullText]

49 **Gnecchi M**, He H, Liang OD, Melo LG, Morello F, Mu H, Noiseux N, Zhang L, Pratt RE, Ingwall JS, Dzau VJ. Paracrine action accounts for marked protection of ischemic heart by Akt-modified mesenchymal stem cells. *Nat Med* 2005; **11**: 367-368 [*RCA*] [PMID: 15812508 DOI: 10.1038/nm0405-367] [FullText]

50 **Lee HJ**, Ko JH, Kim HJ, Jeong HJ, Oh JY. Mesenchymal stromal cells induce distinct myeloid-derived suppressor cells in inflammation. *JCI Insight* 2020; **5**: e136059 [*RCA*] [PMID: 32453713 DOI: 10.1172/jci.insight.136059] [FullText]

51 **Meng SS**, Guo FM, Huang LL, Huang YZ, Xie JF, Yang CS, Qiu HB, Yang Y. mTORC2 Activation Mediated by Mesenchymal Stem Cell-Secreted Hepatocyte Growth Factors for the Recovery of Lipopolysaccharide-Induced Vascular Endothelial Barrier. *Stem Cells Int* 2021; **2021**: 9981589 [*RCA*] [PMID: 34707661 DOI: 10.1155/2021/9981589] [FullText] [Full Text(PDF)]

52 **Birukova AA**, Zagranichnaya T, Fu P, Alekseeva E, Chen W, Jacobson JR, Birukov KG. Prostaglandins PGE(2) and PGI(2) promote endothelial barrier enhancement *via* PKA- and Epac1/Rap1-dependent Rac activation. *Exp Cell Res* 2007; **313**: 2504-2520 [*RCA*] [PMID: 17493609 DOI: 10.1016/j.yexcr.2007.03.036] [FullText] [Full Text(PDF)]

53 **Hezam K**, Wang C, Fu E, Zhou M, Liu Y, Wang H, Zhu L, Han Z, Han ZC, Chang Y, Li Z. Superior protective effects of PGE2 priming mesenchymal stem cells against LPS-induced acute lung injury (ALI) through macrophage immunomodulation. *Stem Cell Res Ther* 2023; **14**: 48 [*RCA*] [PMID: 36949464 DOI: 10.1186/s13287-023-03277-9] [FullText]

54 **Debnath T**, Kim DH, Lim BO. Natural products as a source of anti-inflammatory agents associated with inflammatory bowel disease. *Molecules* 2013; **18**: 7253-7270 [*RCA*] [PMID: 23783459 DOI: 10.3390/molecules18067253] [FullText] [Full Text(PDF)]

55 **Li ZG**, Wang XY, Chang JL, Xie WB, Liu TF, Zhang QL, Deng YJ, Ding YQ. The establishment of supramolecular immunobead real-time PCR and the identification of Cox-2 as a metastasis-related marker in colorectal carcinoma. *Oncol Rep* 2012; **28**: 977-984 [*RCA*] [PMID: 22710400 DOI: 10.3892/or.2012.1867] [FullText]

56 **Wakefield AP**, Ogborn MR, Ibrahim N, Aukema HM. A dietary conjugated linoleic acid treatment that slows renal disease progression alters renal cyclooxygenase-2-derived prostanoids in the Han: SPRD-cy rat. *J Nutr Biochem* 2012; **23**: 908-914 [*RCA*] [PMID: 21940154 DOI: 10.1016/j.jnutbio.2011.04.016] [FullText]

57 **Reverte V**, Tapia A, Moreno JM, Rodríguez L, Salazar F, Llinás MT, Salazar FJ. Renal effects of prolonged high protein intake and COX2 inhibition on hypertensive rats with altered renal development. *Am J Physiol Renal Physiol* 2011; **301**: F327-F333 [*RCA*] [PMID: 21613413 DOI: 10.1152/ajprenal.00110.2011] [FullText]

58 **Majewska A**, Wilkus K, Brodaczewska K, Kieda C. Endothelial Cells as Tools to Model Tissue Microenvironment in Hypoxia-Dependent Pathologies. *Int J Mol Sci* 2021; **22**: 520 [*RCA*] [PMID: 33430201 DOI: 10.3390/ijms22020520] [FullText] [Full Text(PDF)]

59 **Ern C**, Krump-Konvalinkova V, Docheva D, Schindler S, Rossmann O, Böcker W, Mutschler W, Schieker M. Interactions of human endothelial and multipotent mesenchymal stem cells in cocultures. *Open Biomed Eng J* 2010; **4**: 190-198 [*RCA*] [PMID: 21625373 DOI: 10.2174/1874120701004010190] [FullText] [Full Text(PDF)]

60 **Schott NG**, Friend NE, Stegemann JP. Coupling Osteogenesis and Vasculogenesis in Engineered Orthopedic Tissues. *Tissue Eng Part B Rev* 2021; **27**: 199-214 [*RCA*] [PMID: 32854589 DOI: 10.1089/ten.TEB.2020.0132] [FullText]

61 **Wong BW**, Marsch E, Treps L, Baes M, Carmeliet P. Endothelial cell metabolism in health and disease: impact of hypoxia. *EMBO J* 2017; **36**: 2187-2203 [*RCA*] [PMID: 28637793 DOI: 10.15252/embj.201696150] [FullText]

Published by **Baishideng Publishing Group Inc**
7041 Koll Center Parkway, Suite 160, Pleasanton, CA 94566, USA
Telephone: +1-925-3991568
E-mail: office@baishideng.com
Help Desk: https://www.f6publishing.com/helpdesk
https://www.wjgnet.com